

High-power CO₂ laser design “from resonator end mirror to cutting lens focal point”

David Toebaert^{a)}

HACO NV, Oekenestraat 120, 8800 Rumbeke, Belgium

Wybo Wagenaar

Infinite Simulation Systems BV, Lange Bunder 3, 4854 MB Bavel, Netherlands

(Received 13 May 2003; accepted for publication 17 September 2003)

An algorithm is derived that allows calculating all optical parameters relevant to the design of a high-power CO₂ laser, taking into account the practical needs of a flying-optics type of laser cutting machine. The novelty of the approach taken is that the resonator and the beam delivery optics are treated simultaneously, which allows for greater flexibility in design. To begin with, the often-used optical configuration of a stable resonator combined with a beam expander for collimation is modeled and optimized. The remaining focal shift over the cutting table, mainly due to the fact that the part of the beam close to the resonator still has appreciable wavefront curvature variation, is calculated. The resulting function is programmed into the machine CNC, which continuously adjusts the lens position depending on the actual beam length, to compensate for this effect. Next, attention is paid to the well-known problem of changing beam parameters with thermal load of the output coupler. It is found necessary to model both mechanical deformation of the ZnSe window and lensing due to the temperature dependent index of refraction. The former is derived from a finite element model, for the latter, the formula of Miyamoto *et al.* [Proc. SPIE **1276**, 112 (1990)] is used. Finally, as an example of novel resonator designs studied using this approach, the characteristics of an intracavity reflective telescope are determined for two different goals: first, to increase the fundamental mode spot size for the given resonator (and hence to improve beam quality without sacrificing power), and second to preserve beam quality when extra resonator layers are added to increase power. The beam is modeled using the concept of the “embedded Gaussian” and the “complex radius of curvature” due to Siegman [*Lasers* (University Science Books, CA, 1986)].

© 2004 Laser Institute of America.

Key words: laser design, laser beam delivery, laser materials processing

I. INTRODUCTION

During the last few years the interest of the manufacturing community to exploit the advantages of the laser in thick section cutting (minimal heat affected zone, straightness of kerf, flexibility of contouring) has surged.¹ Laser manufacturers have upgraded their existing line of high-power CO₂ lasers (e.g., Trumpf, PRC), or developed entirely new ones (most notably Rofin’s high-power slab laser) to meet the urgent market demand of high power combined with high beam quality.

Nevertheless, market penetration of powers above 4 kW for cutting applications has been slow and hampered with problems, all arising from the difficulty of handling such power in an extended optical train. It is the authors’ belief that this is primarily caused by a lack of integration of the laser and the external optical components, leading to suboptimal solutions for the beam delivery, especially when practical limitations such as aperture size of beam benders and position and size of telescopes are taken into account.

Recently, HACO introduced its newly developed HLT3000 4 kW laser for cutting applications. This develop-

ment, from a research point of view, was an excellent opportunity to reconsider the design process of such a device. When one considers the laser as an integral part of the complete optical train “from resonator end mirror to cutting lens,” one soon realizes that this greatly enhances the flexibility of design. Resonator mirror radii of curvature, outside radius of curvature of the output coupler, position, and curvature of the telescope mirrors can all be optimized relative to the one thing that ultimately counts: beam size and divergence at the cutting lens, and their variation over the cutting table. The remaining focal shift can be compensated for by either having a variable-radius telescope mirror, or a moveable cutting lens. Opting for the moveable cutting lens approach, an extra CNC axis was added to the machine, continuously adjusting the exact lens position to the actual beam length value. That way we were able to maintain cutting quality over the entire travel range of a 4×2 m flat bed cutting machine, especially near the resonator, without any manual intervention, and without relying on operator dependent judgement of cutting quality.

The concept of the “embedded Gaussian” of a higher-order transverse mode laser beam, combined with the elegance of the “complex radius of curvature” approach to beam propagation,² make it possible to tailor a laser to its

^{a)} Author to whom correspondence should be addressed; electronic mail: david.toebaert@skynet.be

application with unprecedented ease. As an example of the method, in Sec. III the complete optical path of the HLT3000 is determined from the simple requirement of collimating the beam over the work plane of the laser-cutting center (LCC), taking into account aperture size of the beam delivery components used.

It is a well-known fact that beam propagation is influenced by the fraction of power absorbed by the optics, heating them, and changing their “design” properties, in particular radii of curvature. In particular the output coupler, due to its low thermal conductivity, is prone to suffer from this problem. To investigate this, a finite-element analysis was carried out at the deformation of the output coupler of the laser by the fractional absorption of the beam passing through it. Also, thermal lensing due to the temperature dependent index of refraction of ZnSe was taken into account by adding an extra lens to the model, whose power can be derived from the analysis by Miyamoto.³ The model was used to compare the results of the “hot” and the “cold” resonator with experimental data for the HLT3000. It was found essential to account for both effects to be able to reproduce the experimental beam spot size variation both close by and far from the resonator.

One particularly interesting feature of the HLT3000, especially in view of the remarks made earlier about the demand for thick-section laser cutting, is its modular design concept. The resonator has been engineered in such a way that it can easily be stacked and optically connected. In order to maintain simultaneously beam quality and power extraction efficiency when adding extra layers to the resonator, it soon followed from the model developed in Sec. II that an extra degree of freedom was necessary in the resonator design. Therefore we investigate the possibility of using a “stable telescopic cavity” (STC) to reach two separate goals: first, for the existing resonator, to increase the fundamental mode spot size and hence to increase the beam quality without sacrificing power, and second, to maintain beam quality regardless of resonator length (and hence beam power).

II. THE MODEL

A. Description of the beam

A lowest-order spherical Gaussian solution to the free-space paraxial wave equation can be completely characterized by its complex radius of curvature $\tilde{q}(z)$, expressed in terms of the physical parameters spot size $w(z)$ and radius of curvature $R(z)$ as

$$\frac{1}{\tilde{q}(z)} = \frac{1}{R(z)} - j \frac{\lambda}{\pi w^2(z)} \quad (1)$$

and the free-space propagation law for $\tilde{q}(z)$

$$\tilde{q}(z_2) = \tilde{q}(z_1) + (z_2 - z_1). \quad (2)$$

In these expressions λ is always the wavelength in the medium in which the beam is propagating, in accordance with the convention established by Siegman.²

Given the complex radius of curvature at a single point along the beam propagation axis z thus completely determines the beam. In particular, at the beam waist z_0

$$\tilde{q}(z_0) = \tilde{q}_0 = j \frac{\pi w_0^2}{\lambda} = j z_R, \quad (3)$$

since at the waist, $R(z_0) = R_0 = \infty$. The quantity z_R is the Rayleigh range of the beam, i.e., at the points $z_0 \pm z_R$ the beam spot size will be $\sqrt{2}w_0$.

Propagation through any paraxial $ABCD$ system can be treated as

$$\tilde{q}_2 = \frac{A \left[\frac{\tilde{q}_1}{n_1} \right] + B}{C \left[\frac{\tilde{q}_1}{n_1} \right] + D}, \quad (4)$$

where the indices 1 and 2 refer to the input and output plane of the $ABCD$ system, and n is the index of refraction at these planes. A full derivation of these formulas, and the theoretical background starting from Maxwell’s equations, can be found in the book by Siegman.² For our purposes we need only remember that at any plane along the beam axis, we can always reconstruct the beam’s radius of curvature and spot size from

$$R(z) = 1/\mathcal{R}(1/\tilde{q}(z)) \quad (5)$$

and

$$w(z) = \sqrt{\lambda/\pi j \mathcal{I}(1/\tilde{q}(z))}, \quad (6)$$

where \mathcal{R} and \mathcal{I} denote the real and imaginary part.

Finally, for a multimode spherical Gaussian beam, i.e., a beam where the transverse field distribution can no longer be described by a Gaussian function, but is modulated by higher-order Hermite (rectangular symmetry) or Laguerre (cylindrical symmetry) polynomials, all the above relationships remain valid provided we multiply the beam spot size by a constant factor M

$$W(z) = M w(z), \quad (7)$$

where we have adopted the convention of using upper-case letters for the spot size of the multimode beam, and lower-case letters for the spot size of the underlying “embedded Gaussian.”⁴ This numerical factor is better known as the “beam quality k ” or M -squared factor:

$$M^2 = 1/k \geq 1. \quad (8)$$

For a theoretically sound value of M^2 it is necessary to use the second-order moment of the transverse intensity distribution of the multimode beam. However, any consistent way of measuring spot size can be used to derive “a” value of M , one needs only keep in mind that the spot sizes produced by using Eqs. (6) and (7) will then always reflect the imperfection of the measuring method.

One particular pitfall in this description of multimode beams relates to the size of the beam in the focal plane of a lens. It is often stated that the effect of a beam quality factor $M^2 > 1$ will be to produce a focal spot M^2 times larger than obtainable with a lowest order Gaussian beam. However, at the lens input, the *embedded Gaussian* spot size will also be M times smaller [Eq. (7)], canceling one factor of M . So, at the focal plane of a lens

- (i) the multimode beam size is M times larger than the embedded Gaussian [Eq. (7)], as it is everywhere; and
- (ii) a *hypothetical* Gaussian beam *with the same spot size and divergence* as the multimode beam *at the lens input* will focus to a spot M^2 times smaller. Do remark that this hypothetical beam cannot be produced by the same resonator that outputs the multimode beam.

So, it is very important to distinguish between hypothetical Gaussian beams used for reference and the unique embedded Gaussian of a multimode beam produced by a particular resonator.

B. Description of the resonator

The resonator is formed by a totally reflecting end mirror at $z = -L_{\text{cav}}$ having a radius of curvature R_{EM} , and the inner reflecting surface of the output coupler at $z=0$ having a radius of curvature R_{OC}^i , where L_{cav} is the physical length of the cavity. The clear aperture of the resonator (which will normally be defined by the diameter of a suitable diaphragm) is denoted by C_{cav} .

Taking the reference plane for the self-consistent calculation of the lowest order mode of this resonator to be just after the end mirror, the round trip $ABCD$ matrix becomes

$$\begin{pmatrix} A & B \\ C & D \end{pmatrix}_{\text{cav}} = \begin{pmatrix} 1 & 0 \\ -2/R_{\text{EM}} & 1 \end{pmatrix} \begin{pmatrix} 1 & L_{\text{cav}}/n_{\text{cav}} \\ 0 & 1 \end{pmatrix} \\ \times \begin{pmatrix} 1 & 0 \\ -2/R_{\text{OC}}^i & 1 \end{pmatrix} \begin{pmatrix} 1 & L_{\text{cav}}/n_{\text{cav}} \\ 0 & 1 \end{pmatrix}, \quad (9)$$

where we have included the possibility of $n_{\text{cav}} > 1$. In the remainder of the text, since we will be dealing with gas lasers, and atmospheric propagation outside of the cavity, we will assume all refractive indices to be unity, except for propagation through the output coupler ($n_{\text{ZnSe}} = 2.40$ at $10.6 \mu\text{m}$).

A self-reproducing radiation field will then have to satisfy $\tilde{q} \equiv (A\tilde{q} + B)/(C\tilde{q} + D)$, which leads to a quadratic equation in $1/\tilde{q}$ and hence two possible solutions, of which, for a geometrically stable resonator, only the one with a negative imaginary part will have finite transverse extent and represent the self-consistent complex radius of curvature of the lowest order Gaussian mode at the end mirror $\tilde{q}(-L_{\text{cav}}) = \tilde{q}_{\text{EM}}$

$$\frac{1}{\tilde{q}_{\text{EM}}} = \frac{D-A}{2B} \mp \frac{1}{B} \sqrt{\left(\frac{A+D}{2}\right)^2 - 1}. \quad (10)$$

Once \tilde{q}_{EM} is known, the spot size and radius of curvature of the wave front at any location between the end mirror and the inside surface of the output coupler can be calculated from Eqs. (2), (5) and (6).

C. Description of the external optical train

The optical path external to the resonator includes propagation through the output coupler, refraction at the ZnSe/ air interface, a telescope to expand and collimate the beam, sev-

eral bending mirrors to take the beam to the cutting head, and finally the cutting lens. Positioning of the cutting lens inside the cutting head is motorized, and is added to the normal X , Y , and Z axes as an extra, “ A ” axis. This feature will be used in Sec. III B when automatically compensating for focal shift due to beam length variation. The A -axis function should not be confused with the mechanical or capacitive devices used to keep the nozzle tip at a fixed distance from the processed sheet, since the latter influences the Z axis only (movement of the cutting head as a whole). What is generally called “autofocus” function, that is, automatically setting focus height for different material types or thicknesses, is also performed by the A axis, but for the purposes of the present article it is essential that the lens position can be adjusted continuously while cutting.

The bending mirrors are flat and as such are not essential to the mathematical description of the beam propagation. They do have special coatings to circularly polarize the beam and protect the laser from back reflections from the processed sheet, but this is irrelevant to the present article’s subject. In the wavelength region of interest the flatness of the mirrors is at least $\lambda/20$, and interferometric tests reveal that this doesn’t change when mounted and/or when cooling water pressure is applied, due to the design of the mirror holder avoiding localized point forces by tightening screws. Finite element analysis of the mirrors under laser radiation also revealed negligible deformation due to heating because of the very low absorption of these coated mirrors ($<0.5\%$, typically 0.3% measured) and the high thermal conductivity of the copper substrate. So, we can safely assume that these mirrors maintain their manufacturer specifications during field use. Moreover, the optical path in the machine is flushed with dried and filtered air, and all traces of organic vapors (mainly oil) are removed by active-carbon filtering, avoiding thermal blooming effects. It would be possible to study the latter using the $ABCD$ matrix for a “duct” with radially varying index, but this is beyond the scope of the current article.

The complete $ABCD$ matrix for propagation from $z = 0$ to the focal plane of the cutting lens can be written as

$$\begin{pmatrix} A & B \\ C & D \end{pmatrix}_{\text{LCC}} = \mathbf{P}_{2f} \mathbf{T}_L \mathbf{P}_{T \rightarrow L} \mathbf{T}_T \mathbf{P}_{\text{OC} \rightarrow T} \mathbf{T}_{\text{OC}}, \quad (11)$$

where

$$\mathbf{T}_{\text{OC}} = \begin{pmatrix} 1 & 0 \\ (1 - n_{\text{ZnSe}})/R_{\text{OC}}^e & 1 \end{pmatrix} \begin{pmatrix} 1 & d_{\text{OC}}/n_{\text{ZnSe}} \\ 0 & 1 \end{pmatrix} \\ \times \begin{pmatrix} 1 & 0 \\ (n_{\text{ZnSe}} - 1)/R_{\text{OC}}^i & 1 \end{pmatrix} \quad (12)$$

propagates the beam through the output coupler.

$\mathbf{P}_{\text{OC} \rightarrow T}$ is free-space propagation to the inlet port of the telescope,

TABLE I. Optical design parameters of a laser source+cutting table combination. All quantities expressed in meters, except for the dimensionless beam quality factor.

Quantity	Description
R_{EM}	Radius of curvature of resonator end mirror (positive: concave, negative: convex)
L_{cav}	Cavity length: distance from end mirror to inside surface of output coupler
R_{OC}^i	Inside radius of curvature of output coupler
d_{OC}	Thickness of output coupler
R_{OC}^e	Outside radius of curvature of output coupler
C_{cav}	Clear aperture of resonator
$d_{OC \rightarrow TM_1}$	Distance from output coupler (outside) to first telescope mirror
R_{TM_1}	Radius of curvature of first (convex) telescope mirror
d_T	Distance between telescope mirrors
R_{TM_2}	Radius of curvature of second (concave) telescope mirror
$d_{OC \rightarrow BM_1}$	Distance from the output coupler (outside) to the first bending mirror on the machine frame without the telescope inserted
$d_{BM_1 \rightarrow L_{00}}$	Distance from the first bending mirror on the machine frame to the focusing lens in its most nearby position
X_{max}	Maximum travel of machine X axis
Y_{max}	Maximum travel of machine Y axis
d_{foc}	Theoretical focal length of cutting lens
C_{BM}	Clear aperture of the bending mirrors used
M	M^2 is the beam quality factor

$$\mathbf{T}_T = \begin{pmatrix} 1 & d_T \\ 0 & 1 \end{pmatrix} \begin{pmatrix} 1 & 0 \\ -2/R_{CC} & 1 \end{pmatrix} \begin{pmatrix} 1 & d_T \\ 0 & 1 \end{pmatrix} \times \begin{pmatrix} 1 & 0 \\ -2/R_{CX} & 1 \end{pmatrix} \begin{pmatrix} 1 & d_T \\ 0 & 1 \end{pmatrix} \quad (13)$$

is the $ABCD$ matrix for the external, off-axis reflective telescope, $\mathbf{P}_{T \rightarrow L}$ is free-space propagation from the outlet port of the telescope to the focusing lens \mathbf{T}_L , and finally the beam is propagated one focal length on both sides of the theoretical focal point by \mathbf{P}_{2f} . The real position of the focal point relative to the focusing lens, and the Rayleigh range, can then be determined numerically.

In the remainder of the text we will use the word “telescope” which is somewhat misleading, since the actual configuration of the “optical device” consisting of two curved mirrors placed slightly off axis in a zig-zag configuration, after optimization, will not necessarily transform a collimated input beam into an expanded, collimated output beam any more. The radii of curvature calculated will take into account the properties of the real beam exiting the laser and so will possibly no longer satisfy

$$\frac{R_{CX}}{2} + d_T = \frac{R_{CC}}{2}.$$

D. The optimization algorithm

Table I lists all parameters relevant to defining the LCC, starting from the resonator end mirror up to the focus of the cutting lens. All of these parameters are, in principle, variable, but some of them may be restricted to a fixed value, or to some fixed range of possible values, depending on physical, mechanical, or other restraints (e.g., when retrofitting a telescope to an existing laser/cutting table combination, size and/or position of the telescope may be restricted, in general

M^2 will be fixed, etc.). The optimization routine starts from a given set of values for all quantities in Table I.

In the first step, the spot size in the resonator is calculated using the formulas of Secs. II A and II B, taking into account the current value of M . This beam is then propagated through the output coupler, the telescope, and finally through the focusing lens, over the entire range of travel of the cutting table. Depending on the size of the laser and the LCC studied, and the radii of curvature used, the number of calculated spot sizes over the entire length of the beam may vary. In practice, for sizes and radii of curvature on the order of meters, a step size of mm has been found more than adequate. In the region of the focal point, however, in order not to lose any detail, a step size of 10 μm was necessary.

Second, the rms deviation of the spot size from the “sollwert,” defined as $87\% \times C_{cav}/2$ for the resonator (see Sec. III A) and C_{BM}/π for the external optical path (not including the distance beyond the focusing lens), is calculated at each point of propagation, and this single number is then transmitted to an optimization routine, which in principle can change *any* parameter from Table I, unless some are artificially restricted, e.g., the beam quality factor can either be fixed, to see what radii of curvature of resonator mirrors is necessary to achieve this particular M^2 , or it can be variable, to investigate what beam quality will be achieved with resonator mirrors that are optimized to achieve a beam spot size as uniform and equal to the intracavity sollwert as possible.

It is very important to note that the resonator and external optical path are optimized simultaneously, and that the criterion for the external optical train ensures less than 1% diffraction ripple in the far field due to cutoff by the external optical components. Also, the optimization routine is interactive in the sense that parameters can be fixed or released at will, in order to study their influence on the beam spot size and propagation behavior.

III. MODEL CALCULATIONS

A. Sample calculation

In order to get a feel for the performance of the algorithm developed and the ways in which it can be used, Figs. 1 and 2 show the results of two model calculations. First, Fig. 1 shows the spot size calculated for a set of values of design parameters as listed in Table II, where the second column (Original value) is taken “from experience.” All parameters were fixed, so the spot size displayed is simply the result of the chosen design parameters, without optimization. The vertical gray lines denote, from left to right: the position of the end mirror, output coupler, first telescope mirror, second telescope mirror, start of travel of the cutting table, and end of travel of the cutting table. The line denoting the output coupler position actually consists of two lines, one for the inside surface and one for the outside, but these are indistinguishable on this scale (thickness of output coupler: 6 mm). The horizontal solid black lines mark the clear aperture of the optical path, which changes when exiting the laser. The horizontal dashed lines denote the value of the beam

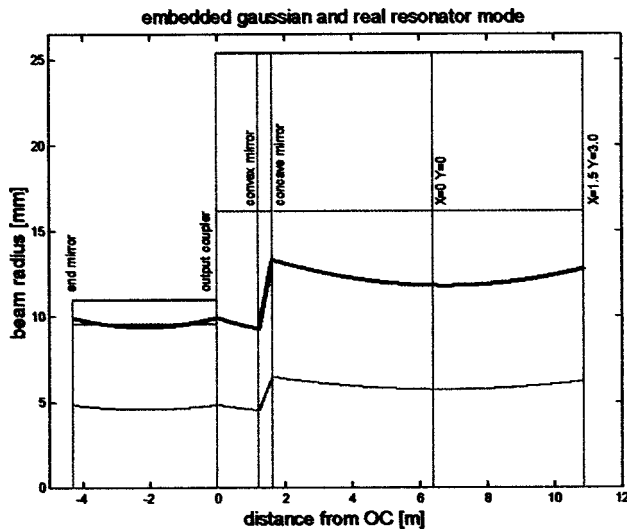


FIG. 1. Original situation of laser/LCC combination. The inside of the output coupler is at $z=0$.

diameter to which the algorithm tries to fit the beam (the sollwert). In this case, since all parameters were fixed except for M , this means that the program calculates the underlying Gaussian for the resonator ($M=1$, curved thin solid line in the figures), which is unique, and then increases M beyond unity until the real beam's $2w$ spot size (curved thick solid line in the figures) fills 87% of the clear aperture of the laser. For a lowest order Gaussian beam, this would mean that its $1/e^2$ points would fit 87% of the clear aperture, which makes good physical sense. We have adopted the same reasoning for higher order modes to determine M . In this particular case, an $M^2=4.22$ is obtained. To test the validity of this approach, Fig. 2 shows the “raw” output from the laser compared to model calculations where all external optics are set to have infinite radius of curvature. It can be seen that the beam diameter variation *outside* of the laser is well fitted by applying the “87% rule” *inside* of the resonator. The shots from the laser were taken by pulsing the power supply, not

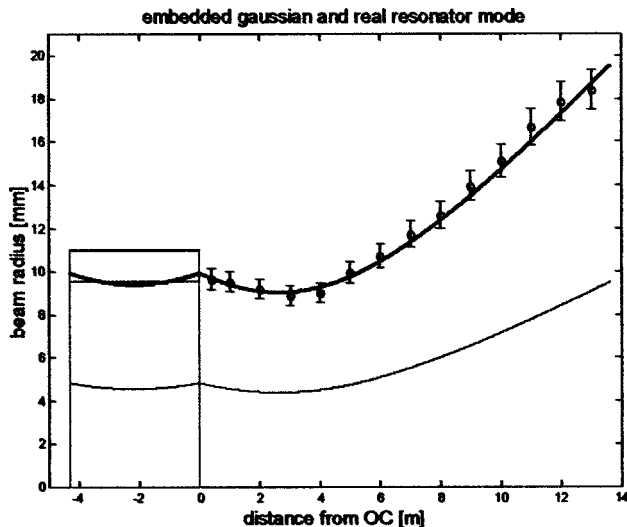


FIG. 2. Comparison of calculated (thick solid line) and measured (o) spot sizes. Error bars are $\pm 5\%$ of the measured value.

TABLE II. Optical design parameters as used in Secs. III A and B. Refer to Table I.

Quantity	Original value	Optimized value Sec. III A	Optimized value Sec. III B (initial)	Optimized value Sec. III B (final)
R_{EM}	20	—	704.72	30
L_{cav}	4.29	—	—	—
R_{OC}^i	20	—	228.77	30
d_{OC}	$6E-3$	—	—	—
R_{OC}^e	7.5	13.1	20.42	10.73
C_{cav}	$22E-3$	—	—	—
$d_{OC \rightarrow TM_1}$	1.225	—	—	—
R_{TM_1}	-1.74	-1.28	-0.933	-0.96
d_T	0.390	—	—	—
R_{TM_2}	2.44	2.00	1.74	1.74
$d_{OC \rightarrow BM_1}$	1.812	—	—	—
$d_{BM_1 \rightarrow L_{00}}$	3.8	—	—	—
X_{max}	1.5	—	2.0	2.0
Y_{max}	3.0	—	6.0	6.0
d_{foc}	0.191	—	—	—
C_{BM}	0.051	—	—	—
M	—	2.056	1.0001	1.850

by using the shutter on a cw operating laser, to avoid thermal deformation of the optics, since the program uses the optical parameters “on the box” and as such cannot take into account changing radii of curvature due to thermal expansion and/or thermal lensing.

The sample calculation (Fig. 1) shows that the cutting lens is underused in that the beam size could be considerably increased (up to the dashed lines for $z>0$) without fear of diffraction effects, leading to a smaller focal spot, and that the beam strikes the cutting lens with a variable divergence from one end of the cutting table to the other, causing a shift in focus position. For this particular case, a change in focus diameter from 0.46 mm at the beginning of the cutting table, to 0.43 mm at the table extremity (in this particular case 1.5 m X travel, 3.0 m Y travel) resulted, at 7.48 in., respectively, 7.56 in. from the input side of the 7.5 in. cutting lens. To improve this situation, the value found for M is fixed, and the values of R_{OC}^e , R_{TM_1} and R_{TM_2} are freed for optimization of the beam delivery. This way, we leave the resonator unchanged (since we are “retrofitting” an existing situation) but try to adapt the external optics. Figure 3 shows the resulting beam diameter variation, and the optimized values are listed in Table II, third column. It can be seen that in this case the useful diameter of the beam delivery components is optimally used. Focus diameter and position is (0.35, 7.48 in.) at $X=Y=0$, and (0.33, 7.52 in.) at $X=1.5$ m, $Y=3.0$ m. A focal shift of 2 mm over the machine travel is thus halved, and the focal spot intensity is more than doubled.

B. Large-range flying optics machines

Currently, the largest dimension flat bed cutting machine produced by HACO has table dimensions of $X=2.0$ m, Y

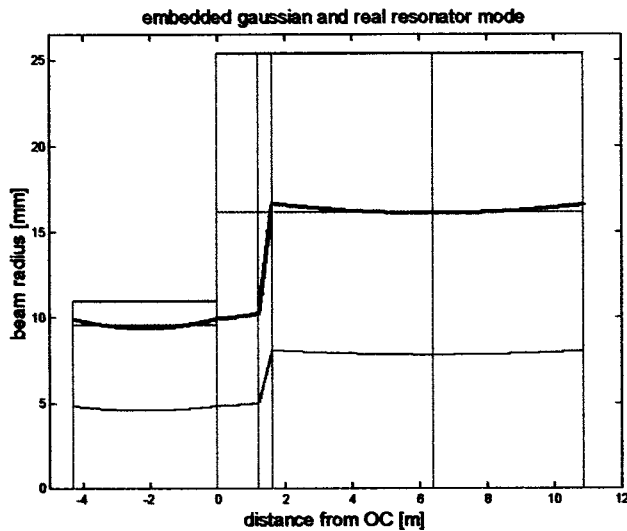


FIG. 3. Optimized solution for a 1.5x3.0 m flatbed LCC.

=6.0 m. The challenge was to adapt the HLT3000 for use over such large distances with the same cutting performance all along the external beam path.

In a first attempt, *all* optical parameters, and M , were set variable. As a consequence, the algorithm increased the end mirror and output coupler's radii of curvature up to a point where the embedded Gaussian filled the resonator completely ($1/e^2 \cong 87\% C_{cav}$, or, alternatively, $M = 1$). This result confirms the approach taken since it is physically quite reasonable. The resulting beam is then so well behaved that the actual spot size never deviates more than 0.1 mm from C_{BM}/π , at any location between the telescope output mirror and the cutting lens, a total distance of almost 13 m. Table II, column 4 lists the obtained design parameters ("initial"). It should be noted that the values for R_{EM} and R_{OC}^i should not be taken literally: the model increases their values until the convergence criterion is reached (fractional change less than 10^{-4}), and so from one calculation to the other the exact values can be different, but in any case are larger than 100 m. Decreasing the convergence criterion (10^{-5} , 10^{-6} , ...) simply increases the radii of curvature further, so that we can conclude that the model is actually trying to reach a plane wave, flat/flat resonator. Of course there remains the practical impossibility of realizing the radii of curvature obtained for the end mirror and the inside surface of the output coupler. Moreover, the resonator would become very prone to alignment deviations. A more practical solution is obtained by limiting both these optics to the largest possible readily available radius, in this case 30 m. The result is listed in Table II, column 5 ("final"). Figure 4 compares the spot size over the machine travel with and without optimization of the combination of the HLT3000 and the external beam path.

Starting from the optimized solution, the location of the focal point relative to the cutting lens is calculated. Figure 5 shows the results, together with a quadratic fit to the data. The location of the focus is expressed as a deviation relative to the focal position for the shortest beam. The deviation of the focal position for the shortest beam from the value "on the box" is compensated for by the operator of the machine

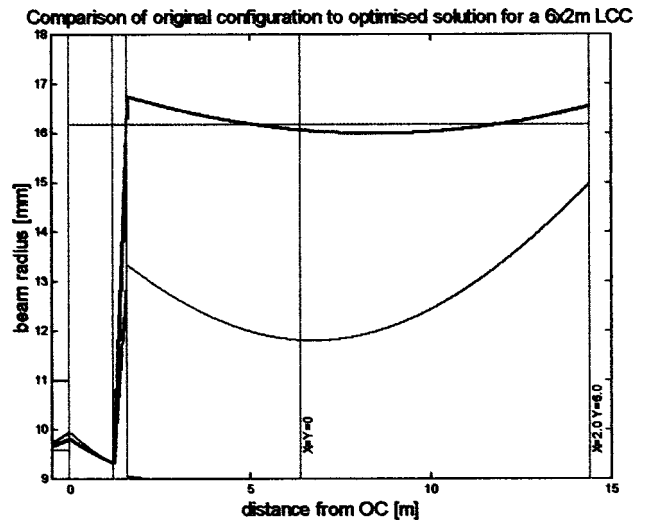


FIG. 4. Spot size variation external to the laser for a 6x2 m flatbed cutting machine. The thick solid line is the optimized solution, the thin solid line shows the propagation behavior of the original configuration. The embedded Gaussians of the two beams are not visible on this zoomed out plot.

prior to cutting when adjusting the lens position for best cutting results. Starting from this point, the A axis then uses the quadratic fit to continuously adapt the lens position to the actual beam length, to ensure that the cutting parameters remain unchanged when the beam length changes. The need for a quadratic fit only arises when suboptimal solutions for the LCC design are used, and the strong variation of focal position near the resonator is more pronounced. As an example we have included the result for the beam of the original configuration of the LCC, Table II, column 2. Note that the total compensation in this case amounts to 2 mm, which would render high-quality cutting over the entire working

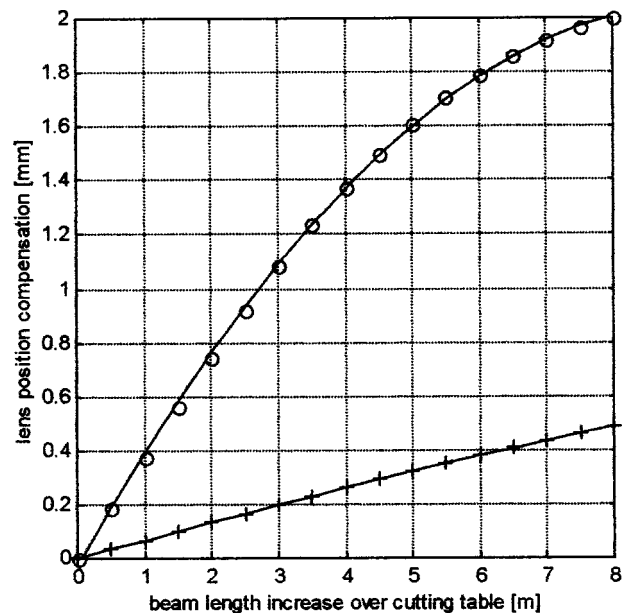


FIG. 5. Parameters for the automatic adjustment of lens position as a function of cutting head position (6x2 m LCC). (o) original configuration, (+) optimized solution.

range of the machine impossible without this automatic adjustment system.

C. The influence of the output coupler

The output coupler is the most vulnerable component of the laser since the beam actually passes through it. Bulk and coating absorption puts in heat, and cooling is hampered by the low thermal conductivity of ZnSe, and the practical limitation of edge cooling.

Two effects need to be taken into account. On the one hand, the window will expand due to heating, which will change the radii of curvature of the optic. On the other hand, the temperature distribution directly translates into an index-of-refraction distribution, adding extra focusing power to the lens $[dn/dT]_{\text{ZnSe}} = 64 \times 10^{-6} (\text{°C})^{-1}$.⁵ The first effect is modeled through a full finite-element analysis of the deformation of the output coupler due to heating, and is described in Sec. IIIC 1. The latter is incorporated into the model by adding a thin lens directly after the output window, whose power is derived from the formula given by Miyamoto as described in Sec. IIIC 2. The combined result is given in Sec. IIIC 3, together with a comparison with experiment.

1. FEA of the output coupler

The temperature distribution and deformation of the ZnSe output coupler in operating conditions is calculated with the ANSYS[®] Finite Element Analysis (FEA) software.⁶ The calculated deformation is used to determine the change in radii of curvature of both sides of the ZnSe output coupler. These curvature changes influence the beam propagation behavior.

In actual operation, the output coupler deforms for two reasons. On the one hand, both sides are coated with a thin film coating consisting of layers of ThF₄ and ZnSe to reach the required reflectivity at the laser wavelength (that is, a certain reflectivity, typically 60%, on the resonator side and an antireflective coating on the outside). These coatings absorb typically 0.125% of the laser power (manufacturer's specification). In the FEA calculations the heat generation in the coatings is applied as an inward heat flux on the surfaces of the ZnSe output coupler. In steady state, this leads to a certain temperature distribution. On the other hand, there is a pressure difference between the output side of the window, which is at atmospheric pressure, and the resonator side, which is typically at 130 mbar absolute pressure. In ANSYS[®] first the temperature distribution is determined and then it is applied, together with the pressure difference, as a structural load to determine the ultimate deformation of the ZnSe output coupler.

In the first step, a geometrical model is defined. Because of axisymmetry, the ZnSe output window is modeled as a two-dimensional rectangle 6 mm wide (window thickness) and 14 mm high (window radius). The outer edge of the window rests on a cooling ring with an inner diameter of 24.5 mm, outer diameter of 28 mm, and a diamond turned surface with a radius of R_{OC}^i , which is maintained at 20 °C. The longer sides of the rectangle are actually curved, with a different curvature on both sides (R_{OC}^i on the resonator side and R_{OC}^e on the outside). For the FEA calculations, this ge-

TABLE III. Material properties as used in the FEA calculations.

	ZnSe	Al
Modulus of elasticity (N/mm ²)	70.3e3	62.053e3
Poisson's ratio	0.28	0.35
Coefficient of thermal expansion (1/°C)	7.57e-6	2.31e-5
Thermal conductivity (W/mm°C)	0.016	0.237

ometry is meshed with a grid of higher-order two-dimensional axisymmetric elements. Thermal contact elements are used to model the heat transfer between the output coupler and the cooling ring. The material properties are listed in Table III. The material properties for ZnSe were taken from the web site of the Institute of Solid State Physics of the Russian Academy of Sciences⁷ since these represent the most recent values we could find (older references tend to differ slightly due to continued improvements in the chemical vapor deposition manufacturing process).

The crucial point in the calculation of the temperature distribution is the correct modeling of the thermal contact conductance at the contact of the ZnSe output coupler and the aluminum cooling ring. This value determines the steady-state temperature rise of the ZnSe optic and hence the amount of deformation. A suitable thermal contact conductance is found by comparing the calculated results with an experimentally measured temperature at the 6 mm side of the ZnSe output coupler.

Figure 6 shows a typical temperature distribution for a laser output power of 3 kW, in a first approximation modeled

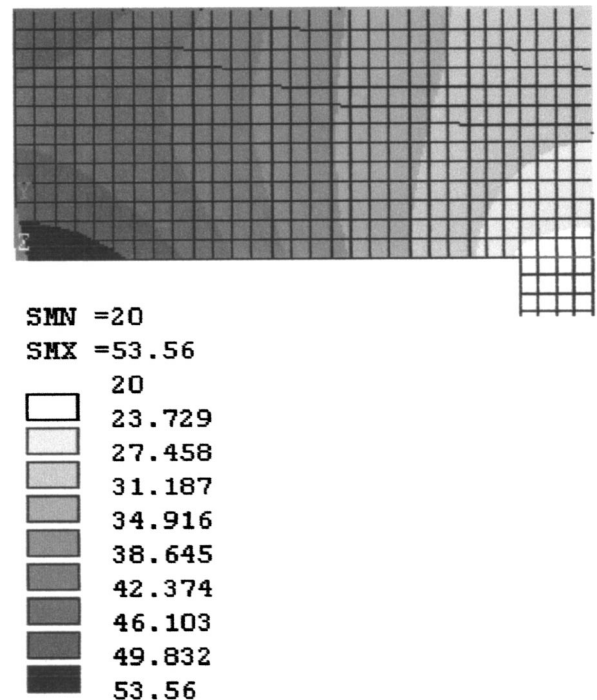


FIG. 6. Typical temperature distribution of the output coupler. Note the higher heating on the resonator side due to the higher power of the intra-cavity beam compared to the exiting beam.

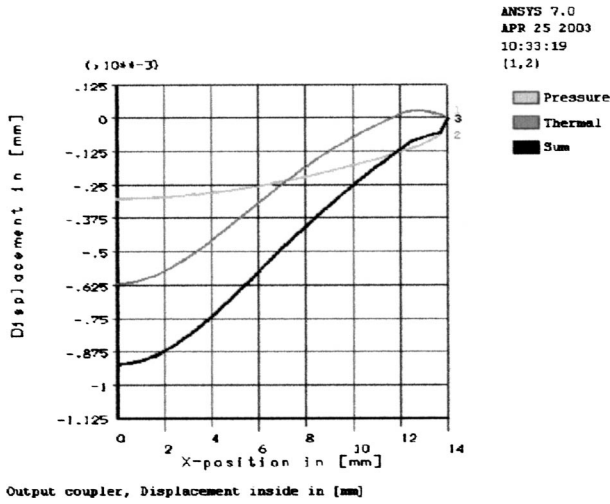


FIG. 7. Expansion of the resonator side of the output coupler due to the combined effect of pressure and heating.

as a Gaussian beam. Figures 7 and 8 show the “bulging” of the optic, from which the resulting radially variable curvature $\kappa(x)$ can be deduced as

$$\kappa = \frac{1}{\rho} = \frac{\partial^2 v(x)/\partial x^2}{[1 + (\partial v/\partial x)^2]^{3/2}}, \quad (14)$$

where ρ is the local radius of curvature and v is the deformed position of the output coupler as a function of the radial coordinate x . For the beam propagation model, this radially variable contribution to the total curvature of the optic is modeled as a spherical deformation by using a best-fit circle through the deformed shape in order to be able to model the effect as a simple change of power of the output coupler “lens,” e.g., in a typical calculation, the output coupler would change from the design values of 20 mcc on the inside, 7.5 mcx on the outside, to 26.5 mcc, 7.2 mcx respectively. These changes are indeed too large to be ignored when designing the optical path of the beam, be it intra- or

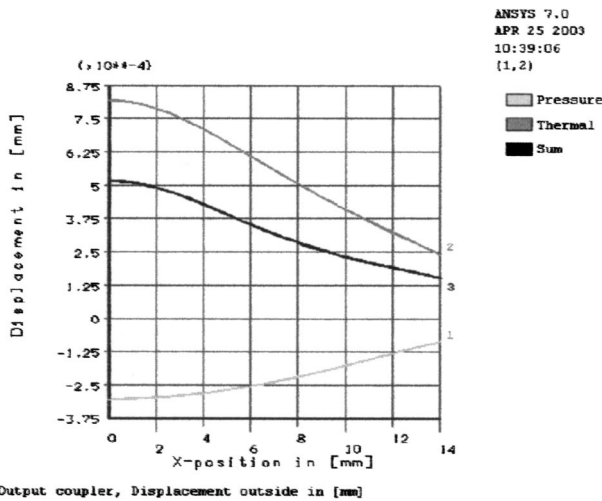


FIG. 8. Expansion of the external (atmospheric) side of the output coupler.

extracavity. The authors are unaware of *ABCD* matrix formulations of optical elements with radially variable curvature, but this would certainly be an improvement to the current model.

2. The effect of thermal lensing

In Ref. 2, it is shown that the power of a ZnSe focusing lens is changed due to heating by an amount Δf given by

$$\Delta f = \frac{AWf^2}{2\pi KR^2} \frac{\partial n}{\partial T}, \quad (15)$$

where A is the optic’s absorption coefficient, W is the incident power, f is the original focal length, K is the thermal conductivity of ZnSe, R is the radius of the assumed incident top-hat power distribution, and the last factor is the coefficient of change of index of refraction with temperature. To achieve this closed formula, a simplified model was used assuming uniform distribution of the heat source in the volume of the optic and no heat losses from the lens surfaces.

In the present case, a real beam of $M^2 > 1$ is incident on a laser output window (basically a very long focus lens) which is actively cooled, and heated by absorption on the surface coatings. Nevertheless, the basic factors of influence on the focal shift should remain the same, so, to a first order approximation, we can write in our notations

$$\Delta f \propto \frac{a_{OC} P_{out}}{W(0)^2} \left[\frac{1}{n-1} \frac{R_{OC}^i R_{OC}^e}{R_{OC}^i + R_{OC}^e} \right]^2, \quad (16)$$

where the proportionality factor is fitted for one particular, experimentally verified situation and found to be 12×10^{-6} . $a_{OC} P_{out}$ represents the total absorbed power and $W(0)$ is the real beam spot size at the output coupler. In this formula, R_{OC}^i should be reckoned negative and R_{OC}^e positive. The model places a thin lens of power $-1/\Delta f$ directly after the output coupler to account for thermal lensing.

The benefit of the current approach is that the fitted proportionality factor consists of material properties only, so the model can be used to study the influence of increasing absorption, increasing power and/or variation of beam spot size at the output coupler on the beam propagation behavior. In fact, for times larger than the thermal equilibration time of the output coupler (experimentally and theoretically found to be about 1 min), the model can calculate the focal shift as a function of incident power and this characteristic can be added to the “geometrical” focus shift of Fig. 5 and compensated for by the *A* axis.

3. Results

Figure 9 shows the calculated results for an output power of 3 kW, leading to calculated radii of curvature $R_{OC}^i = 26.5$ (compared to 20 mcc not deformed), $R_{OC}^e = 7.2$ (7.5 mcx not deformed), and a thermal lens $\Delta f = 35$ m. The general behavior of the beam is very well predicted: close to the resonator the beam focuses more strongly than in “cold” conditions, and at large distances it spreads faster. Except for

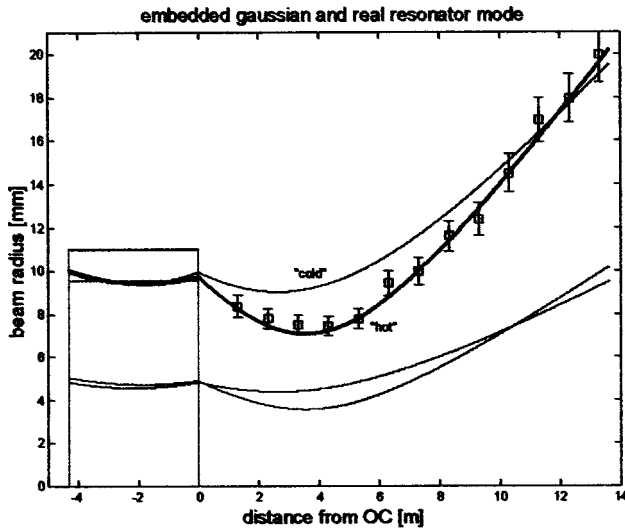


FIG. 9. Modification of the beam propagation by the combined effect of expansion and thermal lensing of the output coupler. The line labeled “cold” is the same as in Fig. 3 and is added for reference, the thick solid line is the calculated result for the loaded resonator together with experimental results for 3 kW laser output (with 5% error bars).

the proportionality factor in Eq. (16), there are no fit parameters at all in the theoretical model, which validates the approach taken.

At first hand, the influence of the thermal lens seems to be negligible compared to the contribution of the mechanical deformation. However, it is impossible to reproduce the experimental beam propagation behavior without modeling both effects. The mechanical deformation primarily determines the stronger focusing near the resonator, while the thermal lens accounts for the faster spreading of the beam at large distances. The model is only capable of reproducing the complete propagation behavior of the beam if both effects are taken into account.

D. The STC

As mentioned earlier, the HLT3000 is completely modular in mechanical design and “stacking” of resonator layers is quite easy. The challenge is to also make the *optical* layout of the resonator “modular,” that’s to say, we want a constant beam quality independent of resonator length. After some trials with the software, it became apparent that the system lacked a degree of freedom to achieve this goal. For that reason, and guided by the excellent results both theoretically and experimentally with the external telescope, we decided to replace the resonator’s end mirror by an intracavity reflective telescope. The idea is to maintain the advantages of a stable resonator (small diffraction effects) and combine them with the advantages of an unstable resonator (large mode volume).

Table IV shows the new list of design variables, now augmented with the internal telescope (first three lines: radius of curvature of convex internal telescope mirror $R_{TM_1}^i$, mirror separation d_T^i , and radius of curvature of concave internal telescope mirror $R_{TM_2}^i$). For compatibility with the standard stable resonator, the cavity length is still reckoned from where normally the end mirror would be, and the inter-

TABLE IV. Optical design parameters for the LCC equipped with a stable telescopic cavity.

Quantity	Optimized value (initial)	Optimized value (single layer)	Optimized value (double layer)
$R_{TM_1}^i$	-0.619	-0.660	-0.607
d_T^i	0.263	—	—
$R_{TM_2}^i$	1.700	1.834	1.723
L_{cav}	4.29	—	8.58
R_{OC}^i	30	∞	∞
d_{OC}	$6E-3$	—	—
R_{OC}^e	10.73	39.83	11.45
C_{cav}	$22E-3$	—	—
$d_{OC \rightarrow TM_1}$	1.225	—	—
R_{TM_1}	-0.96	-0.98	-0.72
d_T	0.390	—	—
R_{TM_2}	1.74	1.78	1.54
$d_{OC \rightarrow BM_1}$	1.812	—	—
$d_{BM_1 \rightarrow L_{00}}$	3.8	—	—
X_{max}	1.5	—	—
Y_{max}	3.0	—	—
d_{foc}	0.191	—	—
C_{BM}	0.051	—	—
M	1.850	1	1

nal telescope is an extension in the negative direction. That way, standard resonators can be studied using the same program by putting $R_{TM_1}^i = R_{EM}$, $d_T^i = 0$, and $R_{TM_2}^i = \infty$. The internal telescope’s dimension was chosen from mechanical restrictions (needed to be interchangeable with the end mirror holder), but care was taken to keep the angle of incidence on the mirrors below 5° to ensure negligible astigmatic effects.

In a first step, all former parameters were fixed at their values attained in Sec. III B for an optimized 6×2 m range LCC, and only the internal telescope mirrors were optimized. This way we could ascertain that it was, in principle, possible to achieve a stable resonator mode with the same beam characteristics as before, but with the end mirror replaced by the internal beam expander. The results are listed in Table IV, second column (initial). The beam produced by this resonator is identical to the one generated by the stable resonator before.

Next, we attempted to achieve unit beam quality by requiring $M=1$ and adapting $R_{TM_1}^i$, $R_{TM_2}^i$, and R_{OC}^i . Table IV, column 3 (single layer) shows the resulting optical configuration of the resonator, together with the adapted external optical path, since the beam now has a modified propagation behavior. Figure 10 shows the beam spot size variation, which is perfectly matched to the sollwert throughout the optimization region. It should be noted that *all* optics, internal and external to the resonator, were optimized simultaneously, taking about 5 min on a desktop PC with a 750 MHz processor.

Finally, in view of the remarks made earlier, the same performance should be attainable with a longer resonator (read: higher-power laser). To test this, we doubled the resonator length and reran the simulation. Table IV, column 4 (“double layer”) lists the results, graphed in Fig. 11. Achieving such a result by starting off with an estimated configura-

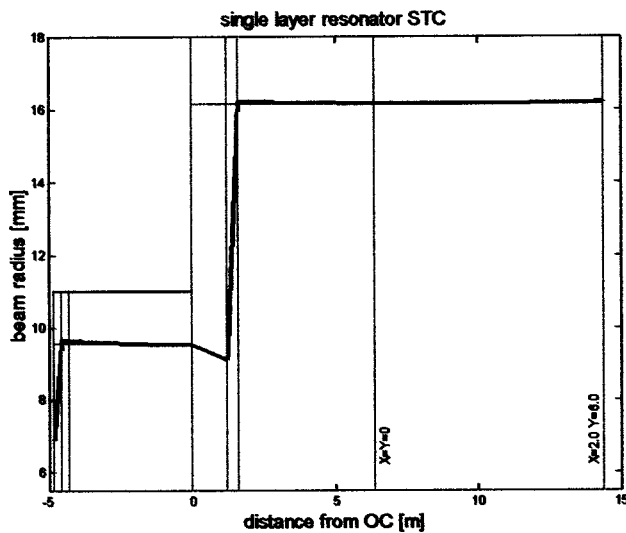


FIG. 10. Unit beam quality STC mode with external optics optimized for a 6×2 m flatbed LCC. The first three vertical lines denote the position of first and second internal expander mirrors, and the position where normally the end mirror would be. The beam radius is indistinguishable from its sollwert throughout the optimization region. Mind the expanded view of the vertical axis.

tion and experimentally optimizing would be almost impossible in view of the delicate interrelation of all parameters. Figure 12 shows a schematic layout of the cavity of this laser, the HLT6000, which is currently under construction and has a projected output power of 7 kW. At this power level the optimization of the beam characteristics over a 6×2 m bed will be greatly facilitated by the findings of this article.

Experimental verification of the feasibility of using the STC for mode improvement and/or mode conservation when increasing resonator length and hence output power is yet to be performed. A prototype has already been tested on a single-layer resonator with positive results. In contrast to what we expected, adjustment sensitivity was only

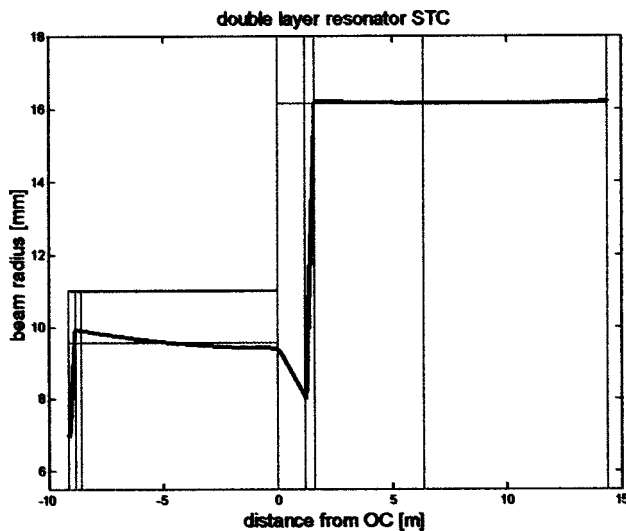


FIG. 11. Unit beam quality STC mode in a double-layer resonator constructed by stacking two layers of the HLT3000.

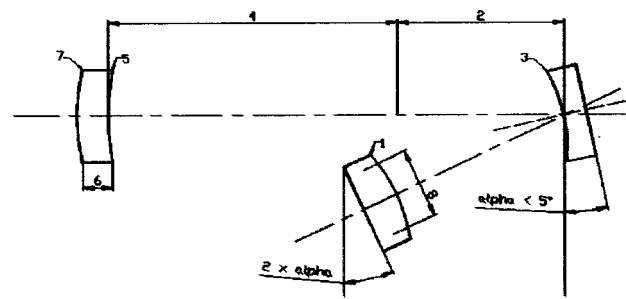


FIG. 12. Schematic layout of the STC (not to scale). Referring to Table IV, the numbers indicated on the figure denote: (1) R_{TM1}^i ; (2) d_T^i ; (3) R_{TM2}^i ; (4) L_{cav} ; (5) R_{OC}^i ; (6) d_{OC} ; (7) R_{OC}^o ; (8) C_{cav} . Note that for intracavity use, the convex mirror has to be inclined at double the angle of the concave one to have zero angle of incidence and project the beam back onto the output coupler.

slightly higher than for a single end mirror, and mode shape stability was unaltered. We did notice a reduction in mode order which couldn't be accounted for. We attribute this to the fact that we didn't use the exact values of telescope mirror radii of curvature calculated, but rather the most nearby ones available "off the shelf." Full experimental verification will take place after completion of construction of the HLT6000.

IV. CONCLUSIONS

In this article we present an elegant, easy-to-use, versatile model that is capable of predicting laser beam propagation over the complete optical path of a laser cutting machine, including the resonator itself.

Several features typical of high-power laser cutting centers of the flying-optics type are studied using this approach. The focal shift due to the varying wave front curvature over the cutting table range is determined and compensated for by using an extra CNC axis to adjust cutting lens height to the position on the cutting table. This way, constant cutting quality is achieved over a range of 4×2 m without manual intervention, and without using operator-dependent judgement of cutting quality. Next, the problem of spot size variation due to output coupler heating is modeled. It is found that it is essential to model both the mechanical deformation of the optic (bulging) as well as the thermal lens effect (temperature dependent index of refraction) to be able to reproduce the beam propagation behavior both at short and long distances from the output coupler. Finally, the possibilities of using an intracavity beam expander to either increase beam quality or preserve it when stacking resonator layers to increase power are discussed theoretically.

The model presented can be used to determine beam quality factors for given resonators, design new resonators, fit telescopes to existing lasers, calculate the necessary focal shift compensation curves for flying optics machines, compensate for thermally induced focal shift, ... and finally even to design complete laser cutting centers from scratch, including the resonator.

- ¹K. Laughlin, "Turning up the power: using lasers to cut thick plate," *Fabricator* (December 1999) (<http://www2.thefabricator.com/Fabricator/Fabricator.htm>).
- ²A. E. Siegman, *Lasers* (University Science Books, CA, 1986).
- ³I. Miyamoto, H. Nanba, and H. Maruo, "Analysis of thermally induced optical distortion in lens during focusing high power CO₂ laser beam," *CO₂ Lasers and Applications II* [Proc. SPIE **1276**, 112 (1990)].
- ⁴*The Physics and Technology of Laser Resonators*, edited by D. R. Hall and P. E. Jackson (IOP Ltd., London, 1989).
- ⁵H. E. Reedy and G. L. Herrit, "Comparison of GaAs and ZnSe for high power CO₂ laser optics," *High Power CO₂ Laser Systems and Applications* [Proc. SPIE **1020**, 180 (1988)].
- ⁶www.ansys.com
- ⁷www.issp.ac.ru